Application of Volume of Fluid Method for the Droplet Modelling in Microfluidic Channels

Emil Grigorov

***Abstract* — We used the volume-of-fluid (VOF) method to investigate the droplet formation regime and its transition in a square microfluidic flow-focusing device. Droplet shape, size, and its formation frequency were examined in a three-dimensional numerical simulation. The results were evaluated through examination of the regimes of droplet formation and the formation of droplet of given size as a function of different parameters. Comparison of the simulation results with preexisting experimental data from the literature showed good agreement, validating the VOF method.**

***Index Terms* — microfluidics, droplets, modelling, CFD, Volume of Fluid**

I. Introduction

In recent years, microfluidic devices have emerged as a novel tool for the realization of different biological and medical processes. The decreased reagents volumes, usually in the micro/nanoliters range, can significantly reduce reaction times and energy consumption for a certain process [1]. Droplet-based microfluidics, which encapsulates different chemical or biological compounds into individual picolitre-droplets, allows the isolation of reactions from their surroundings, protecting them from unwanted mixing and allowing better control over a massive number of independent reactions. These small microreactors have allowed an easily implementable and relatively cheap approach for a broad range of processes including cell lysis [2], DNA purification [3], polymerase chain reaction (PCR) [4] and many more. Therefore, understanding the mechanisms behind the droplet generation is crucial for the efficiency of a droplet-based microfluidic systems.

Droplets formation usually occurs when two immiscible liquids intersect each other. The process is achieved either by active (using valves or electric fields) or by passive (using pressure-driven flow and the channel geometry) methods. The specific design of the microfluidic channels makes it possible for an aqueous phase, usually water, to be sheared by another continuous phase (hydrocarbon oils, fluorocarbon oils etc. [5]) and produce uniform-sized drops. Different geometry designs are possible, the most utilized in the praxis are: T-junction [6-7], flow-focusing [8-9], or co-flowing [10]. Figure 1 shows the three variants.

The next few paragraphs should contain the authors' current affiliations, including current address and e-mail. E. G. Author is with Faculty of German Engineering Education and Industrial Management (FDIBA), Technical University of Sofia, "Sveti Kliment Ohridski" 8, 1756, Bulgaria (e-mail: egrigorov@fdiba.tu-sofia.bg).

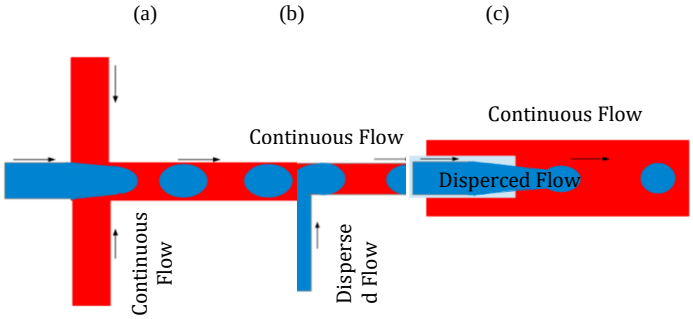

Fig. 1. Different geometrical designs for the droplet formation in microfluidic channels: (a) Flow-focusing, (b) T-Junktion, (c) Co-flow.

For the design of microfluidic devices operating in droplet flow regime, prior knowledge of droplet size, shape, formation frequency or pressure drop are essential. Several experimental studies have already investigated the mechanisms behind droplet generation in microfluidic channels [11-15]. Those measurements give an adequate information about the needs of a certain experimental setup; however, it is not possible generally to include the influence of all possible effective parameters of the system. Another feasible way to collect in advanced this information for a new setup is by utilizing a predictive CFD model and interpreting the influences of some fluid properties on the droplet breakup. Few numerical studies on droplet-based microfluidics were carried out in the past years utilizing different numerical techniques (for example level set (LS) [16] or Lattice Boltzmann method (LBM) [17]). All these techniques show the usefulness of CFD methods as a valuable predictive tool.

In this article we investigate numerically the droplet formation in a flow-focusing microfluidic channel by utilizing the volume of fluid (VOF) method. First, we validate our results with data from another numerical study from the literature. In a second part, using the same geometry, we make a parameter study which extends beyond the range of [19]. In this part, new flow regimes of the droplet-based microfluidics are considered. The velocity of the continuous phase and its influence on the droplet formation are investigated and analyzed.

TABLE 1
PHYSICAL PROPERTIES OF CONTINUES AND DISPERSED PHASES

Fluid	Density - ρ [kg/m^3]	Viscosity - μ [mPas]
Water	995,4	0,89
Oil (Octane 2,5+5% span 80)	689,9	0,53

https://doi.org/10.47978/TUS.2021.71.04.001

II. Mathematical Model, Geometrical Setup, Boundary Conditions and Numerical Details

In the present study three-dimensional simulations of droplet formation in a flow-focusing geometry as shown in Fig.1 are carried out. The two immiscible fluids, water and oil as well as their interface, are modelled by the Volume of fluid (VOF) method. In this method, following the Eulerian principle, the fluid flow is treated as a continuum. A phase fraction parameter, α, is used to indicate the presence of each phase at every location of the domain. Fluid properties such as viscosity and density are smoothed and the surface tension force is distributed near the interface as a body force in the Navier-Stokes equations.

With this, the system of coupled partial differential equation consists of the continuity equation (Eqn.1) the momentum balance equation (Eqn. 2), and the phase fraction equation for α (Eqn. 3) becomes:

$$\frac{\partial \rho}{\partial t} + \nabla . \rho \mathbf{U} = 0 \quad (1)$$

$$\frac{\partial (\rho \mathbf{U})}{\partial t} + \nabla . (\rho \mathbf{U}\mathbf{U}) = -\nabla p + \nabla . (\mu [\nabla \mathbf{U} + \nabla \mathbf{U}^{T}]) + \mathbf{F_s} \quad (2)$$

$$\frac{\partial (\rho \alpha)}{\partial t} + \nabla . (\rho \alpha \mathbf{U}) = 0 \quad (3)$$

In the equations above, **U** is the velocity vector field and p is the pressure field. $\mathbf{F_S}$ represents the surface tension force and is defined as shown in Eqn. 4:

$$\boldsymbol{F_s} = \sigma \kappa (\nabla \alpha) \quad (4)$$

where κ is curvature ($\kappa = \nabla . (\nabla \alpha / |\nabla \alpha|)$). Only one such transport equation (Eqn. 3) needs to be solved since the volume fraction of the other phase can be inferred from the constraint:

$$\alpha_c + \alpha_d = 1 \quad (5)$$

where the index '*c*' stands for continuous and '*d*' for dispersed phase. The viscosity μ and the density ρ are based on the weighted average of the phase fraction:

$$\mu = \alpha \mu_C + (1 - \alpha) \mu_D \quad (6)$$

$$\rho = \alpha \rho_C + (1 - \alpha) \rho_D \quad (7)$$

In order to verify the results from the utilized numerical model, we considered a geometry of a flow-focusing microchannel, already investigated by Sontti et al [19]. The lengths and dimensions of the square cross-section, the inlet and outlet channels are presented in Figure 2.

The continuous phase (water/water + 40% glycerol) is introduced through the two side channels and the dispersed phase (oil: octane +2,5% SPAN 80) is entered from the main (central) channel. Table 1 summarizes the physical properties of the two oil-water systems considered for the verification of the model and the later calculations in our work. As in [19], the information is obtained from the experimental results of Yao et al. [20]. All the measurements were conducted under atmospheric pressure conditions and room temperature (25±1,5 °C).

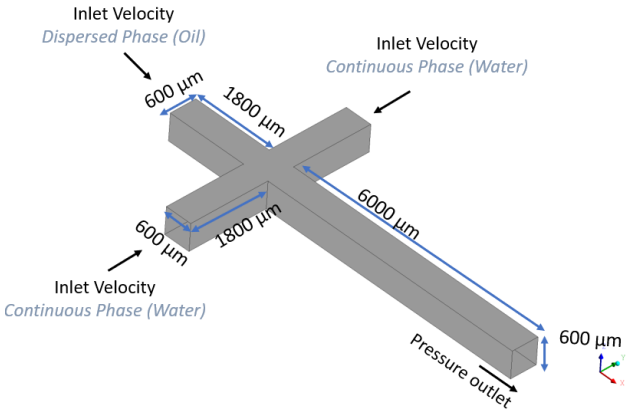

Fig. 2. Model geometry, dimensions and boundary conditions for the present verification - following Sontti et al. [19].

A finite volume method based CFD solver from ANSYS Fluent 16 with the implemented Volume of Fluid technique is used to solve the system of time-dependent partial differential equations. For the boundary conditions, constant velocity block profile was utilized for both continuous and dispersed phase inlets. We set α =1 at the inlet of the dispersed phase and α = 0 at the inlet of the continuous phase. The walls of the channels were considered as fully wetted by the continuous phase, therefore the contact angle was set as zero at the walls. No slip boundary conditions are applied at the walls. Pressure boundary was specified at the outlet of the main channel. Table 2 summarizes the varied boundary conditions for each case investigated. The inlet velocity of the dispersed phase (oil) was kept constant at u_d = 0,0185 m/s for all 4 cases. Water was utilized as a continuous phase, the surface tension coefficient between the two fluids is taken from [20] and equals 5,37 mN/m.

TABLE 2

Boundary conditions varied for the investigation of droplet formation in the present work

Case	Inlet velocity of the continuous phase, [m/s]
1	0,0185
2	0,00925
3	0,0370
4	0,0740

Making use of the mesh sensitivity analysis made by Sontti et al. [19], we considered a near wall mesh refinement with a first row of thickness of 6 µm and continuing with a 13% size increase towards the middle of the channel. The middle elements reach 35 µm length size, and an overall of 390 000 elements are required for the hexahedral equidistant mesh. A variable time step and a fixed Courant number (Co = 0,25) were considered for solving equations 1-3.

III. Verification

As mentioned before, in order to examine the efficiency of the VOF model, first a verification of the results with the work of Santi et al. [19] is made. The authors utilized a combination of the VOF and LV (Level Set) methods. Compared to the pure VOF model their CLSVOF (Coupled Level Set and Volume of Fluid method) technique showed more accurate methodology in capturing the interface

between the two fluids and a close agreement with the experimental work of Wu et al. [21]. A detailed comparison between the VOF and the CLSVOF models is made by Keshavarzi et al. [22]. For our verification, cases 1 and 2 from Table 3 are considered and compared with identical simulations from [19].

Figure 3 shows the comparison of the droplet formation in the middle plane of the domains through time in the two studies for case 1. It can be seen that both results have very close time scales regarding the generation of oil (blue) in water (red) droplets. First, the so-called filling stage (0,020s – 0,040s) is observed, where the dispersed phase is injected into the main channel. At some point the growing oil-front blocks the flow from the side channels causing the upstream pressure to increase until it reaches a value where the continuous phase begins to squeeze the interface [23]. In the second, so called, necking stage (0,040s – 0,055s) the dispersed phase (oil) is still being injected into the droplet at a constant flow rate, while the neck collapses. The collapse accelerates triggering the last pinch-off stage, where the droplet detaching occurs (around 0,060s). The three stages described above form, the so-called dripping regime in a flow-focusing microfluidics device [24].

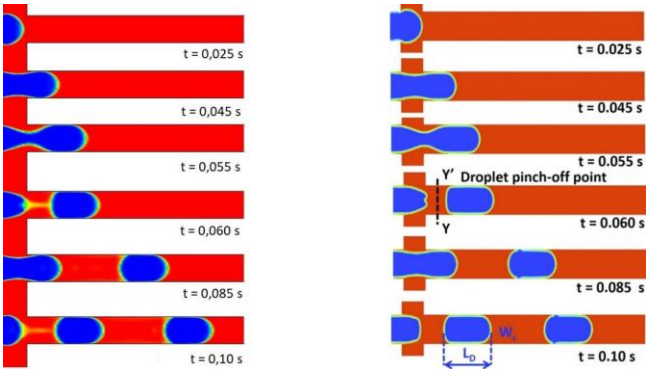

Fig. 3. Comparison of the droplet formation in our work (left) and Sontti et al. [19] (right) for case 1. Results from [19] are reproduced with permission

A quantitative comparison of the two cases considered is also carried out and summarized in Table 3. The nondimensional droplet length with respect to channel width (= L_D/Wc) and the droplet volume V_D are utilized for this purpose. For the calculation of V_D we use Equation 8, with f standing for the frequency of droplet formation in Hertz and Q_C being the volume flow rate of the continuous phase:

$$V_D = \frac{Q_C}{f} \tag{8}$$

TABLE 3

QUANTITATIVE COMPARISON OF THE RESULTS IN OUR WORK WITH THE WORK OF SONTTI ET AL

	Water/Oil		
Parameter	**Our work**	**Santi et al. [19]**	**Rel. error [%]**
L_D/W	1,92	2,12	9,5
Droplet Volume [nL]	257	298	13,6

A relative difference of around 13-14% is observed for the volume of the generated droplets and around 10% for their length with respect to the channel width. This is in a reasonably good agreement with the CLSVOF method presented in [19], as the VOF technique often tends to smear the step profile of the interface over several mesh cells because of numerical diffusion, as it has been demonstrated in [22].

IV. RESULT DISCUSSION

In order to understand better how droplet size for the flow-focusing microdroplet generator could be controlled more precisely, three additional cases with varied continuous phase velocities (at constant dispersed flow rate of u_d = 0,0185 m/s) were carried out, extending the range of simulated values by Sontti et al [19]. Figure 4 shows the three-dimensional iso-surfaces of the droplets for varied continuous phase inlet velocity. It can be seen, that with increasing u_c, droplet size decreases and formation frequency increase. It is worth mentioning also that with increasing velocity value of the continuous phase a long-suspended column of the disperse fluid flows at the tube (for example Figures 4 (d) a, so called jetting regime [27]. Here, the shear from the continuous phase in the channel results in the elongation of the inner dispersed stream, and undulations that appear on the interface between the two fluids get carried downstream (so called Rayleigh-Plateau instability). In this regime, Garstecki et al [28] demonstrated that breakup of drops does not occur due to shear stress but due to the pressure drop across the emerging drop.

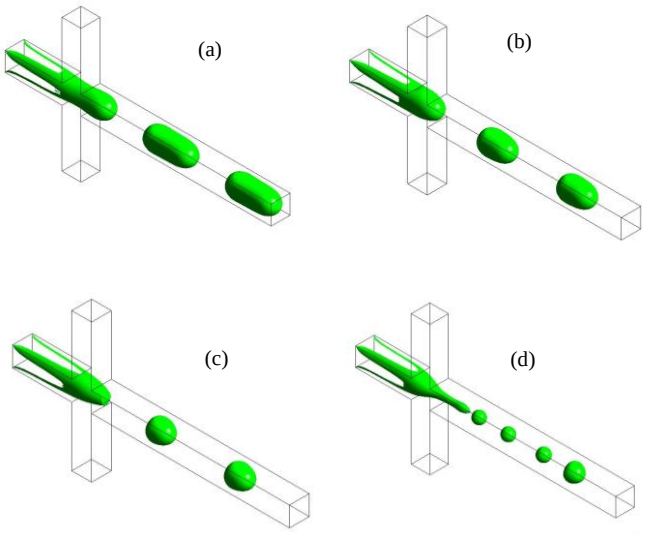

Fig. 4. A three dimensional iso surface of droplet evolution for (a) uc = 0,00925 m/s (b) = 0,0185 m/s (c) = 0,0370 m/s (c) = 0,0740 m/s

The effect of the surface tension force gets also noticeable in Figure 4. Higher continuous phase velocities disrupt the tendency of the surface tension to create few big droplets with less surface energy. Smaller droplets are therefore connected with bigger curvature radii and larger differences in the pressure jumps between the inside and the outside of a single droplets.

Figure 5 shows the development of the nondimensional droplet length as a function of the velocity ratio of the two fluids. It is important to mention that these results are shown for a constant flow ratio (velocity) of the dispersed phase at 0,0185 m/s. The 'cutting' shear force on the droplets

increases at higher velocity ratios, making the length of the droplet to decrease and thus, as shown in Figure 4 droplet size decreases at higher velocity ratios. The results are in good agreement with the results shown in [19].

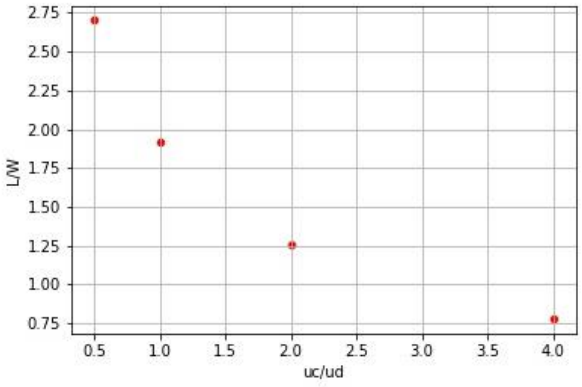

Fig. 5. The nondimensional droplet length as a function of the velocity ratio at u_d = 0,0185 m/s.

Figure 6 on the other hand shows that smaller droplets creation occurs at faster frequencies. Naturally, there is a lower limit to the size a particular device can achieve and this is based upon the physical size and individual geometry of that particular device. A noticeable frequency jump is observed for the last 4th case, where the jetting regime in the channels is present.

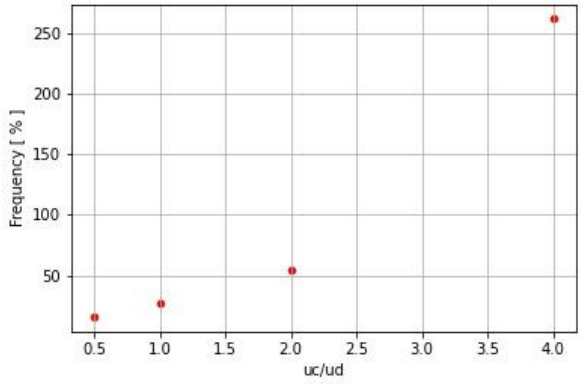

Fig. 6. The frequency of droplet generation as a function of the velocity ratio at u_d = 0,0185 m/s.

These correlations are in good agreement with the results shown in Figure 7, in which the drops volume is shown as a function of the velocity ratio. Again, for the case with the highest velocities, a visible volume decline is visible.

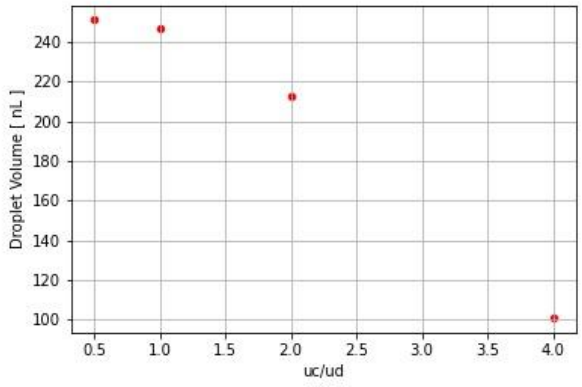

Fig. 7. The droplet volume as a function of the velocity ratio at u_d = 0,0185 m/s.

V. Conclusion

In this work the droplet generation in a flow-focusing microfluidic device has been investigated. The continuous phase (water/water + 40 % glycerol) was introduced through the two side channels and the dispersed phase (oil: octane +2,5% SPAN 80) was entered from the main channel. For all simulations the VOF method was utilized. In the first part, a verification of the technique with the results from Sontti et al [19] has been made. A good agreement between the two works, with maximum differences of 13% is found which are attributed mainly to the different numerical techniques. This part shows that the VOF method is a reliable technique for the simulation and prediction of droplet generation in a flow-focusing channels.

In the second part of the present investigation, the range of the velocity of the continuous phase from the work of Sontti et al. [19], was extended in order to see the dependency of the flow regime from the velocity. It was found that at higher flow rates (velocities), smaller drops at higher frequencies were formed.

As an outlook, a further investigation of the role of other parameters (fluid properties, surface tension) on the transition drop formation regimes and droplet size should be investigated.

References

[1] N. Nguyen, S. Wereley, Fundamentals and Applications of Microfluidics; Artech House Publishing: Norwood, MA, USA, (2007)
[2] Grigorov, E.; Kirov, B. Marinov, M.B. Galabov, V. Micromachines 12, 498 (2021), https://doi.org/10.3390/mi12050498
[3] Xu, Y. Zhang, Z. Su, Z. Zhou, X. Han, X. Liu, Q. Micromachines, 11, 187 (2020), https://doi.org/10.3390/mi11020187
[4] Madhusudan B. K.; Sanket G. Eng. Res. Express 2 042001 (2020), https://doi.org/10.1088/2631-8695/abd287
[5] N. Shembekar, C.Chaipan, R.Utharala, C.A.Merten, Lab Chip, 16, 1314-1331 (2016), https://doi.org/10.1039/C6LC00249H
[6] T. Thorsen , R. W. Roberts , F. H. Arnold, S. R. Quake , Phys. Rev. Lett., 86 , 4163 —4166 (2001), https://doi.org/10.1103/PhysRevLett.86.4163
[7] W. Zeng and H. Fu, IEEE 8th International Conference on Fluid Power and Mechatronics (FPM), 1190-1196 (2019)
[8] S. L. Anna , N. Bontoux and H. A. Stone , Appl. Phys. Lett., 82, 364 —366 (2003), https://doi.org/10.1063/1.1537519
[9] L. Yobas , S. Martens, W. L. Ong, N. Ranganathan , Lab Chip, 6, 1073 —1079 (2006), https://doi.org/10.1039/b602240e
[10] C. Cramer , P. Fischer, E. J. Windhab , Chem. Eng. Sci., 59, 3045-3058 (2004), https://doi.org/10.1016/j.ces.2004.04.006
[11] Mazutis, L., Gilbert, J., Ung, W. Nat Protoc 8, 870–891 (2013), https://doi.org/10.1038/nprot.2013.046
[12] M. A. Bijarchi, A. Favakeh, S. Alborzi, M. B. Shafii, Sensors and Actuators B: Chemical, 329, (2021), https://doi.org/10.1016/j.snb.2020.129274
[13] Y. Zhang, L. Wang, Nanoscale and Microscale Thermophysical Engineering, 13:4, 228-242 (2009), https://doi.org/10.1080/15567260903276999
[14] W. Lan, S. Li, G. Luo, Chem.Eng. Sc., 134, 76-85, (2015), https://doi.org/10.1016/j.ces.2015.05.004
[15] Y. Lu, T. Fu, C. Zhu, Y. Ma, H. Z. Li, Chem. Eng. Sc., 105, 213-219, (2014), https://doi.org/10.1016/j.ces.2013.11.017
[16] Lan, W.; Li, S.; Wang, Y.; Luo, G. Ind. Eng. Chem. Res., 53, 4913 (2014), https://doi.org/10.1021/ie403060w
[17] Y. Li, M. Jain, Y. Ma, Nandakumar, Soft Matter, 11, 3884 (2015), https://doi.org/10.1039/C5SM00252D
[18] Gupta, A.; Matharoo, H. S.; Makkar, D.; Kumar, R. Comput. Fluids, 100, 218 (2018), https://doi.org/10.1016/j.compfluid.2014.05.023
[19] S. Sontti, A. Atta, Ind. Eng. Chem. Res. 59, 9, 3702–3716 (2020), https://doi.org/10.1021/acs.iecr.9b02137
[20] C. Yao, Y. Liu, C. Xu, S. Zhao, G. Chen, AIChE J., 64, 346 (2018), https://doi.org/10.1002/aic.15889
[21] L. Wu, M. Tsutahara, L. S. Kim, M. Ha, Int. J. Multiphase Flow, 34, 852 (2008), https://doi.org/10.1016/j.ijmultiphaseflow.2008.02.009

[22] G. Keshavarzi, G. H. Yeoh, T. Barber, The Journal of Computational Multiphase Flows. 5(1), 43-55 (2013), https://doi.org/10.1260/1757-482X.5.1.43
[23] P. A. Romero, A.R. Abate, Lab Chip, 12, 5130-5132 (2012), https://doi.org/10.1039/c2lc40938k
[24] X. Chen, T. Glawdel, N. Cui, Microfluid Nanofluid 18, 1341–1353 (2015), https://doi.org/10.1007/s10404-014-1533-5
[25] J. D. Wehking, M. Gabany, L. Chew, Microfluid Nanofluid 16, 441–453 (2014), https://doi.org/10.1007/s10404-013-1239-0
[26] R. Sh. Abiev, Chemical Engineering Science,Volume **174**, p.403-412, (2017), https://doi.org/10.1016/j.ces.2017.09.041
[27] N. M. Kovalchuk, M. Sagisaka, K. Steponavicius, Microfluid Nanofluid, **23,** 103 (2019), https://doi.org/10.1007/s10404-019-2269-z
[28] X. Chen, T. Glawdel, N. Cui, Microfluid Nanofluid 18, 1341–1353 (2015), https://doi.org/10.1007/s10404-014-1533-5
[29] J. K. Nunes, S.S. H. Tsai, J. Wan, H.A. Stone, H. A. (2013). Journal of Physics D: Applied Physics, 46(11), 114002 (2013), https://doi.org/10.1088/0022-3727/46/11/114002